Journal club

February 3, 2015

Spin-Orbit Coupling and the Optical Spin Hall Effect in Photonic Graphene

A. V. Nalitov, G. Malpuech, H. Terças, and D. D. Solnyshkov, Phys. Rev. Lett. **114**,026803 (2015)

Tibor Sekera

UNI
BASEL

Outline

Outline

- Photonic graphene

Outline

- Photonic graphene
- Tight-binding description

Outline

- Photonic graphene
- Tight-binding description
- Numerical simulation

Outline

- Photonic graphene
- Tight-binding description
- Numerical simulation
- Conclusions

Photonic graphene

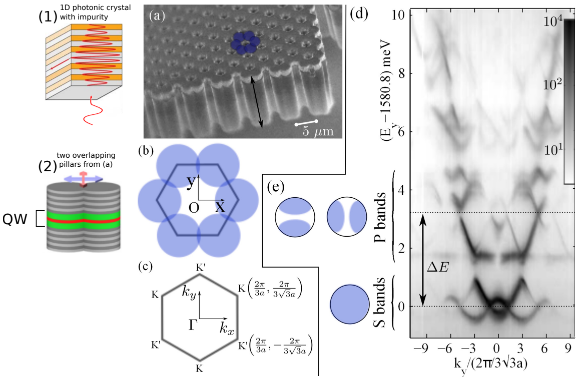

Figure : a) Scanning electron microscope image of a corner of the microstructure. One hexagon of pillars is underlined with blue disks. The dark arrows show the growth axis of the cavity. The overlap between pillars is sketched in (b). (c) First BZ. (d) Measured momentum space energy resolved photoluminescence at $k_x = -2\pi/3a$, under nonresonant low-power excitation. (e) Sketch of the real space distribution of S and P modes in a single pillar.

D. D. Solnyshkov, et al., Phys. Rev. Lett. **112**, 116402 (2014)

Photonic graphene

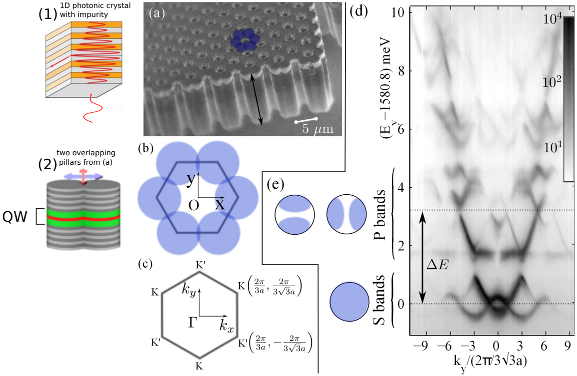

- In the real experimental setup (Fig.(a)), there is a strong coupling between the localized cavity photons and quantum well excitons.

D. D. Solnyshkov, et al., Phys. Rev. Lett. **112**, 116402 (2014)

Photonic graphene

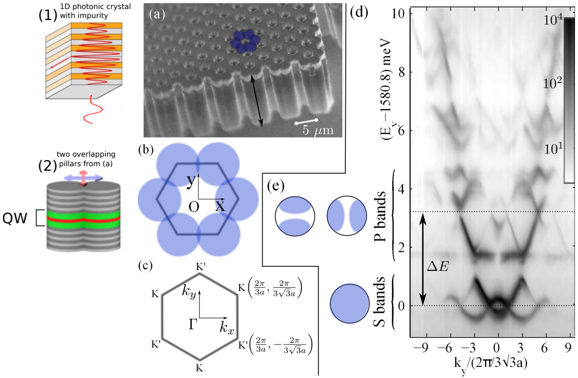

- In the real experimental setup (Fig.(a)), there is a strong coupling between the localized cavity photons and quantum well excitons.
- Hence the particles that really tunnel are "exciton-polaritons" (bound state of photon and exciton), however, authors claim that the model applies for both in the regime they consider.

D. D. Solnyshkov, et al., Phys. Rev. Lett. **112**, 116402 (2014)

Tunneling amplitudes

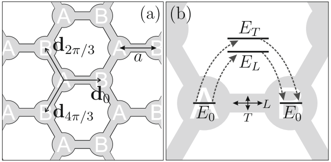

- In linear polarization basis $\{L, T\}$:

$$\langle A, L|\hat{V}|B, L\rangle \equiv E_L = -J - \delta J/2,$$
$$\langle A, T|\hat{V}|B, T\rangle \equiv E_T = -J + \delta J/2,$$
$$\langle A, L|\hat{V}|B, T\rangle = \langle A, T|\hat{V}|B, L\rangle = 0.$$

The energy difference δJ is due to "longitudal-transversal (L-T) splitting" of the linearly polarized modes.[1]

[1] G. Panzarini, et al., Phys. Rev. B 59, 5082 (1999)

Tunneling amplitudes

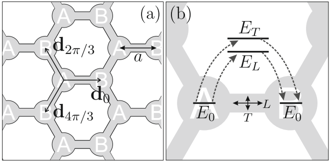

- In linear polarization basis $\{L, T\}$:

$$\langle A, L|\hat{V}|B, L\rangle \equiv E_L = -J - \delta J/2,$$
$$\langle A, T|\hat{V}|B, T\rangle \equiv E_T = -J + \delta J/2,$$
$$\langle A, L|\hat{V}|B, T\rangle = \langle A, T|\hat{V}|B, L\rangle = 0.$$

The energy difference δJ is due to "longitudal-transversal (L-T) splitting" of the linearly polarized modes.[1]

- In circular polarization basis $\{+, -\}$:

$$\langle A, \pm|\hat{V}|B, \pm\rangle = -J, \quad \langle A, +|\hat{V}|B, -\rangle = -\delta J e^{-2i\varphi},$$

where φ is the angle between the link and the horizontal axis.

[1] G. Panzarini, et al., Phys. Rev. B 59, 5082 (1999)

Tight-binding description

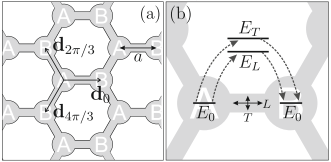

- state of the particle in the i-th unit cell is described by bispinor $\Phi_i = \left(\Psi_A^+, \Psi_A^-, \Psi_B^+, \Psi_B^-\right)_i^{\mathrm{T}}$, with $\Psi_{A(B)}^{\pm}$ being the wave function describing polarization ($\pm$) and sublattice A(B).

Tight-binding description

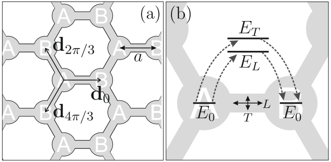

- state of the particle in the i-th unit cell is described by bispinor $\Phi_i = \left(\Psi_A^+, \Psi_A^-, \Psi_B^+, \Psi_B^-\right)_i^{\mathrm{T}}$, with $\Psi^{\pm}_{A(B)}$ being the wave function describing polarization ($\pm$) and sublattice A(B).

- Using the translational symmetry, one can block-diagonalize $\langle i|\hat{H}|j\rangle$ via Fourier transform $\Phi_i \to \Phi_{\mathbf{k}}$

Tight-binding description

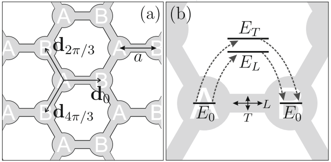

- 4x4 block in $\Phi_{\mathbf{k}}$ basis is

$$\mathrm{H}_{\mathbf{k}} = \begin{pmatrix} 0 & \mathrm{F}_{\mathbf{k}} \\ \mathrm{F}^{\dagger}_{\mathbf{k}} & 0 \end{pmatrix}, \quad \mathrm{F}_{\mathbf{k}} = -\begin{pmatrix} f_{\mathbf{k}} J & f^{+}_{\mathbf{k}} \delta J \\ f^{-}_{\mathbf{k}} \delta J & f_{\mathbf{k}} J \end{pmatrix},$$

where complex coefficients $f_{\mathbf{k}}, f^{\pm}_{\mathbf{k}}$ are defined by:

$$f_{\mathbf{k}} = \sum_{j=1}^{3} \exp(-\mathrm{i}\mathbf{k}\mathbf{d}_{\varphi_j}), \quad f^{\pm}_{\mathbf{k}} = \sum_{j=1}^{3} \exp(-\mathrm{i}\left[\mathbf{k}\mathbf{d}_{\varphi_j} \mp 2\varphi_j\right]),$$

and $\varphi_j = 2\pi(j-1)/3$ is the angle between the horizontal axis and the direction to the jth nearest neighbor of a type-A pillar.

Rewriting $\mathrm{H}_{\mathbf{k}}$

- Rewriting $\mathrm{H}_{\mathbf{k}}$ in terms of Pauli matrices $\boldsymbol{\sigma}$ and $\mathbf{s}$ corresponding to sublattice A and B and polarization degrees of freedom, they obtained

$$\begin{aligned} H_{\mathbf{k}}^{(0)} &= -J\sigma_{+} f_{\mathbf{k}} + h.c. \qquad \leftarrow \text{graphene-like term}, \\ H_{\mathbf{k}}^{\mathrm{SO}} &= -\delta J \sigma_{+} \otimes \left(f_{\mathbf{k}}^{+} s_{+} + f_{\mathbf{k}}^{-} s_{-} \right) + h.c., \end{aligned}$$

where $\sigma_{\pm} = (\sigma_x \pm \mathrm{i}\sigma_y)/2$ and $s_{\pm} = (s_x \pm \mathrm{i} s_y)/2$.

Dispersion from the tight-binding model

- Diagonalizing $\mathrm{H}_{\mathbf{k}}$ they obtained 4 dispersion curves:

$$2(E_{\mathbf{k}}^{\pm})^2 = 2|f_{\mathbf{k}}|^2 J^2 + \left(|f_{\mathbf{k}}^{+}|^2 + |f_{\mathbf{k}}^{-}|^2\right)\delta J^2 \pm$$
$$\pm\sqrt{(|f_{\mathbf{k}}^{+}|^2 - |f_{\mathbf{k}}^{-}|^2)^2 \delta J^4 + 4|f_{\mathbf{k}} f_{\mathbf{k}}^{+*} + f_{\mathbf{k}}^{*} f_{\mathbf{k}}^{-}|^2 J^2 \delta J^2}.$$

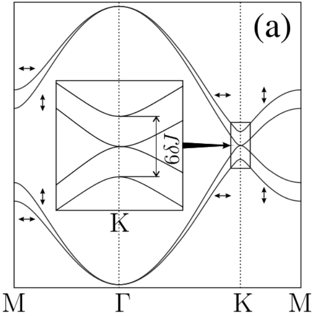

Figure : (a) gapples dispersion in region $\delta J/J \ll qa \ll 1$

Low energy approximation around K and K′ points

- Expanding terms $H_{\mathbf{k}}^{(0)}$ and $H_{\mathbf{k}}^{\mathrm{SO}}$ around $\mathbf{q} = \mathbf{k} - \mathbf{K}$ and isolating $\mathbf{q}-$independent and -depend parts $H_{\mathbf{K}}^{\mathrm{SO}}$ and $H_{\mathbf{q}}^{\mathrm{SO}}$ they obtained

$$H_{\mathbf{q}}^{(0)} = \hbar v_F \left(\tau_z q_x \sigma_x + q_y \sigma_y \right), \tag{1}$$

$$H_{\mathbf{K}}^{\mathrm{SO}} = \Delta \left(\tau_z \sigma_y s_y - \sigma_x s_x \right), \tag{2}$$

$$H_{\mathbf{q}}^{\mathrm{SO}} = \frac{\Delta a}{2} \left[s_x (\tau_z q_y \sigma_y - q_x \sigma_x) - s_y (\tau_z q_x \sigma_y + q_y \sigma_x) \right] \tag{3}$$

where $v_F = 3Ja/(2\hbar)$, $\Delta = 3\delta J/2$ and τ_z equals $+1(-1)$ for K(K′) valleys.

Low energy approximation around K and K′ points

- Expanding terms $H^{(0)}_{\mathbf{k}}$ and $H^{\mathrm{SO}}_{\mathbf{k}}$ around $\mathbf{q} = \mathbf{k} - \mathbf{K}$ and isolating $\mathbf{q}-$independent and -depend parts $H^{\mathrm{SO}}_{\mathbf{K}}$ and $H^{\mathrm{SO}}_{\mathbf{q}}$ they obtained

$$H^{(0)}_{\mathbf{q}} = \hbar v_F \left(\tau_z q_x \sigma_x + q_y \sigma_y\right), \tag{1}$$

$$H^{\mathrm{SO}}_{\mathbf{K}} = \Delta \left(\tau_z \sigma_y s_y - \sigma_x s_x\right), \tag{2}$$

$$H^{\mathrm{SO}}_{\mathbf{q}} = \frac{\Delta a}{2} \left[s_x(\tau_z q_y \sigma_y - q_x \sigma_x) - s_y(\tau_z q_x \sigma_y + q_y \sigma_x)\right] \tag{3}$$

where $v_F = 3Ja/(2\hbar)$, $\Delta = 3\delta J/2$ and τ_z equals $+1(-1)$ for K(K′) valleys.

- For $\delta J = 0$ only the first graphene-like term (1) is non-zero.

Low energy approximation around K and K′ points

- Expanding terms $H_{\mathbf{k}}^{(0)}$ and $H_{\mathbf{k}}^{\mathrm{SO}}$ around $\mathbf{q} = \mathbf{k} - \mathbf{K}$ and isolating $\mathbf{q}-$independent and -depend parts $H_{\mathbf{K}}^{\mathrm{SO}}$ and $H_{\mathbf{q}}^{\mathrm{SO}}$ they obtained

$$H_{\mathbf{q}}^{(0)} = \hbar v_F \left(\tau_z q_x \sigma_x + q_y \sigma_y\right), \tag{1}$$

$$H_{\mathbf{K}}^{\mathrm{SO}} = \Delta \left(\tau_z \sigma_y s_y - \sigma_x s_x\right), \tag{2}$$

$$H_{\mathbf{q}}^{\mathrm{SO}} = \frac{\Delta a}{2} \left[s_x(\tau_z q_y \sigma_y - q_x \sigma_x) - s_y(\tau_z q_x \sigma_y + q_y \sigma_x)\right] \tag{3}$$

where $v_F = 3Ja/(2\hbar)$, $\Delta = 3\delta J/2$ and τ_z equals $+1(-1)$ for K(K′) valleys.

- For $\delta J = 0$ only the first graphene-like term (1) is non-zero.

- Term (3), $H_{\mathbf{q}}^{\mathrm{SO}} \sim \delta J.(qa)$, is "the smallest" of them in considered regions $\delta J, qa \ll 1$, so we forget it in what follows

Low energy approximation around K and K′ points

- Expanding terms $H^{(0)}_{\mathbf{k}}$ and $H^{\mathrm{SO}}_{\mathbf{k}}$ around $\mathbf{q}=\mathbf{k}-\mathbf{K}$ and isolating $\mathbf{q}-$independent and -depend parts $H^{\mathrm{SO}}_{\mathbf{K}}$ and $H^{\mathrm{SO}}_{\mathbf{q}}$ they obtained

$$
\begin{aligned}
H^{(0)}_{\mathbf{q}} &= \hbar v_F \left(\tau_z q_x \sigma_x + q_y \sigma_y\right), && (1)\\
H^{\mathrm{SO}}_{\mathbf{K}} &= \Delta \left(\tau_z \sigma_y s_y - \sigma_x s_x\right), && (2)\\
H^{\mathrm{SO}}_{\mathbf{q}} &= \frac{\Delta a}{2}\left[s_x(\tau_z q_y \sigma_y - q_x \sigma_x) - s_y(\tau_z q_x \sigma_y + q_y \sigma_x)\right] && (3)
\end{aligned}
$$

  where $v_F = 3Ja/(2\hbar)$, $\Delta = 3\delta J/2$ and τ_z equals $+1(-1)$ for K(K′) valleys.

- For $\delta J = 0$ only the first graphene-like term (1) is non-zero.

- Term (3), $H^{\mathrm{SO}}_{\mathbf{q}} \sim \delta J.(qa)$, is “the smallest“ of them in considered regions $\delta J, qa \ll 1$, so we forget it in what follows

- Term (2) is dominant in region $qa \ll \delta J/J$ and is responsible for band splitting at K,K′ points $\Rightarrow$ effective photon mass $m^* = (2c\hbar^2\delta J)/(3a^2J^2)$.

$$
\begin{aligned}
H_{\mathbf{q}}^{(0)} =& \hbar v_F \left(\tau_z q_x \sigma_x + q_y \sigma_y \right), && (1) \\
H_{\mathbf{K}}^{\mathrm{SO}} =& \Delta \left(\tau_z \sigma_y s_y - \sigma_x s_x \right), && (2)
\end{aligned}
$$

- In region $\delta J/J \ll qa \ll 1$, term (2) is a perturbation to the polarization independent graphene-like term (1).

$$H_{\mathbf{q}}^{(0)} = \hbar v_F \left(\tau_z q_x \sigma_x + q_y \sigma_y\right), \quad (1)$$

$$H_{\mathbf{K}}^{\mathrm{SO}} = \Delta \left(\tau_z \sigma_y s_y - \sigma_x s_x\right), \quad (2)$$

- In region $\delta J/J \ll qa \ll 1$, term (2) is a perturbation to the polarization independent graphene-like term (1).
- It splits its linearly polarized eigenstates in energy, therefore can be interpreted as an interaction with an in-plane effective magnetic field (in considered region of parameters).

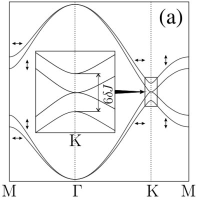

Figure : (a) gapples dispersion in region $\delta J/J \ll qa \ll 1$

Effective in-plane magnetic field

$$H_{\mathbf{K}}^{\mathrm{SO}} = \Delta \left(\tau_z \sigma_y s_y - \sigma_x s_x \right) \tag{2}$$

- If one restricts the state space by fixing the sublattice (positive/negative energies, $c = \pm$) and valley (K,K$'$, $\tau_z = \pm$), term (2) can be transformed into

Effective in-plane magnetic field

$$H_{\mathbf{K}}^{\mathrm{SO}} = \Delta \left(\tau_z \sigma_y s_y - \sigma_x s_x \right) \tag{2}$$

- If one restricts the state space by fixing the sublattice (positive/negative energies, $c = \pm$) and valley (K,K′, $\tau_z = \pm$), term (2) can be transformed into

$$\langle c, \tau_z | H_{\mathbf{K}}^{\mathrm{SO}} | c, \tau_z \rangle \equiv H_c^{\mathrm{SO}} = - \Delta c \tau_z \left(q_x s_x - q_y s_y \right) / q, \tag{4}$$

  where $|c, \tau_z\rangle$ is one of four eigenstates of graphene-like term (1).

- (4) is "symmetry allowed Dresselhaus-like emergent field"

Effective in-plane magnetic field

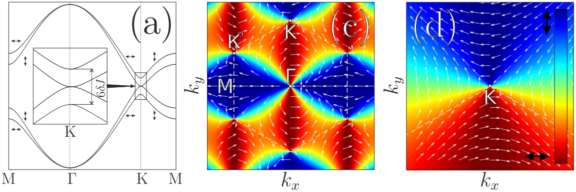

$$H_c^{\mathrm{SO}} = -\Delta c \tau_z \left(q_x s_x - q_y s_y\right)/q \tag{4}$$

- the effective field (4) doesn't open the gap, but leads to the appearence of massive particles

Effective in-plane magnetic field

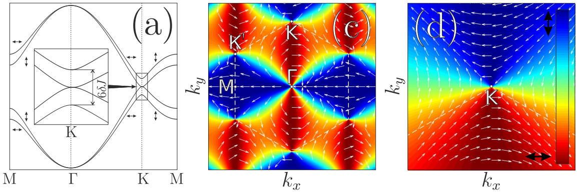

$$H_c^{\mathrm{SO}} = -\,\Delta c \tau_z \left(q_x s_x - q_y s_y\right)/q \tag{4}$$

- the effective field (4) doesn't open the gap, but leads to the appearence of massive particles
- moreover, (4) splits the degenerate Dirac cones by $3\delta J$, Fig.(a)

Effective in-plane magnetic field

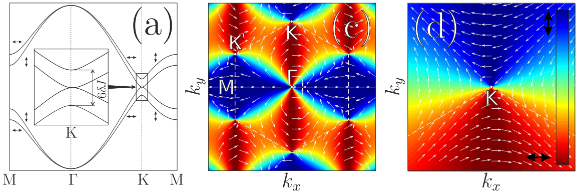

$$H_c^{\mathrm{SO}} = -\Delta c \tau_z \left(q_x s_x - q_y s_y\right)/q \tag{4}$$

- the pseudospin (polarization of particles) pattern of the lowest energy eigenstate reflects the effective field acting on the particles (white arrows), because the pseudospin aligns with this field Fig.(c),(d)

Effective in-plane magnetic field

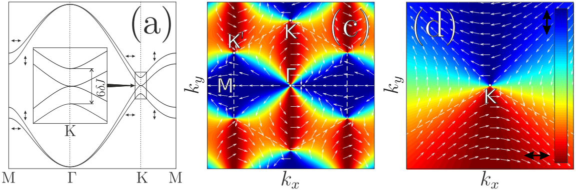

$$H_c^{\mathrm{SO}} = -\Delta c \tau_z \left(q_x s_x - q_y s_y \right) / q \tag{4}$$

- the pseudospin (polarization of particles) pattern of the lowest energy eigenstate reflects the effective field acting on the particles (white arrows), because the pseudospin aligns with this field Fig.(c),(d)
- in Fig.(c) it can be seen that the effective field near K and K′ has opposite sign

Optical spin Hall effect (OSHE)

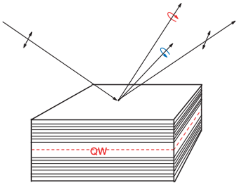

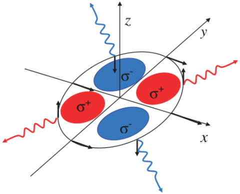

- The best evidence of the presence of a spin-orbit coupling inducing an effective magnetic field of a specific symmetry is the optical spin-Hall effect[2]

[2] Phys. Rev. Lett. **95**, 136601 (2005)

Optical spin Hall effect (OSHE)

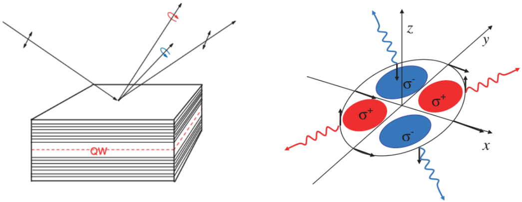

- The best evidence of the presence of a spin-orbit coupling inducing an effective magnetic field of a specific symmetry is the optical spin-Hall effect[2]

Theoretical prediction:

- The resonant excitation around the Γ point with linearly polarized light should lead to the radial expansion of wavepacket and formation of four spin domains (in real space).

[2] Phys. Rev. Lett. **95**, 136601 (2005)

Optical spin Hall effect (OSHE)

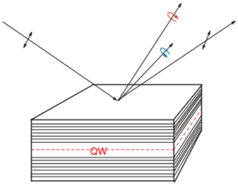

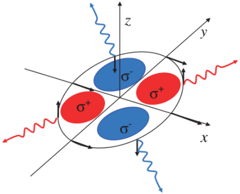

- The best evidence of the presence of a spin-orbit coupling inducing an effective magnetic field of a specific symmetry is the optical spin-Hall effect[2]

Theoretical prediction:

- The resonant excitation around the Γ point with linearly polarized light should lead to the radial expansion of wavepacket and formation of four spin domains (in real space).

- Close to the K and K' points only the two spin domains (in real space) should form.

[2] Phys. Rev. Lett. **95**, 136601 (2005)

Numerical simulation

- To check the validity of TB approximation and observability of the OSHE in real samples, they solve the equation of motion for photonic spinor

$$i\hbar\frac{\partial\psi_\pm}{\partial t} = -\frac{\hbar^2}{2m}\Delta\psi_\pm + U\psi_\pm - \frac{i\hbar}{2\tau}\psi_\pm + \tag{5}$$
$$+\beta\left(\frac{\partial}{\partial x} \mp i\frac{\partial}{\partial y}\right)^2\psi_\mp + P_0 e^{-\frac{(t-t_0)^2}{\tau_0^2}} e^{-\frac{(\mathbf{r}-\mathbf{r}_0)^2}{\sigma^2}} e^{i(\mathbf{k}\mathbf{r}-\omega t)}$$

where:

$\psi(r) = \psi_+(r), \psi_-(r)$ are the two circular components of the photon wave function (polariton polarization)

Numerical simulation

- To check the validity of TB approximation and observability of the OSHE in real samples, they solve the equation of motion for photonic spinor

$$i\hbar\frac{\partial\psi_\pm}{\partial t} = -\frac{\hbar^2}{2m}\Delta\psi_\pm + U\psi_\pm - \frac{i\hbar}{2\tau}\psi_\pm + \tag{5}$$
$$+\beta\left(\frac{\partial}{\partial x} \mp i\frac{\partial}{\partial y}\right)^2\psi_\mp + P_0 e^{-\frac{(t-t_0)^2}{\tau_0^2}} e^{-\frac{(\mathbf{r}-\mathbf{r}_0)^2}{\sigma^2}} e^{i(\mathbf{kr}-\omega t)}$$

where:

$\psi(r) = \psi_+(r), \psi_-(r)$ are the two circular components of the photon wave function (polariton polarization)
m is the cavity photon (polariton) mass

Numerical simulation

- To check the validity of TB approximation and observability of the OSHE in real samples, they solve the equation of motion for photonic spinor

$$i\hbar\frac{\partial\psi_\pm}{\partial t} = -\frac{\hbar^2}{2m}\Delta\psi_\pm + U\psi_\pm - \frac{i\hbar}{2\tau}\psi_\pm + \tag{5}$$
$$+\beta\left(\frac{\partial}{\partial x} \mp i\frac{\partial}{\partial y}\right)^2\psi_\mp + P_0 e^{-\frac{(t-t_0)^2}{\tau_0^2}} e^{-\frac{(\mathbf{r}-\mathbf{r}_0)^2}{\sigma^2}} e^{i(\mathbf{k}\mathbf{r}-\omega t)}$$

where:

$\psi(r) = \psi_+(r), \psi_-(r)$ are the two circular components of the photon wave function (polariton polarization)
m is the cavity photon (polariton) mass
U describes the honeycomb lattice

Numerical simulation

- To check the validity of TB approximation and observability of the OSHE in real samples, they solve the equation of motion for photonic spinor

$$i\hbar\frac{\partial\psi_\pm}{\partial t} = -\frac{\hbar^2}{2m}\Delta\psi_\pm + U\psi_\pm - \frac{i\hbar}{2\tau}\psi_\pm + \tag{5}$$
$$+\beta\left(\frac{\partial}{\partial x} \mp i\frac{\partial}{\partial y}\right)^2\psi_\mp + P_0 e^{-\frac{(t-t_0)^2}{\tau_0^2}} e^{-\frac{(\mathbf{r}-\mathbf{r}_0)^2}{\sigma^2}} e^{i(\mathbf{kr}-\omega t)}$$

where:

$\psi(r) = \psi_+(r), \psi_-(r)$ are the two circular components of the photon wave function (polariton polarization)
m is the cavity photon (polariton) mass
U describes the honeycomb lattice
τ is the lifetime of photon (polariton)

Numerical simulation

- To check the validity of TB approximation and observability of the OSHE in real samples, they solve the equation of motion for photonic spinor

$$i\hbar\frac{\partial\psi_\pm}{\partial t} = -\frac{\hbar^2}{2m}\Delta\psi_\pm + U\psi_\pm - \frac{i\hbar}{2\tau}\psi_\pm + \qquad (5)$$
$$+\beta\left(\frac{\partial}{\partial x} \mp i\frac{\partial}{\partial y}\right)^2\psi_\mp + P_0 e^{-\frac{(t-t_0)^2}{\tau_0^2}} e^{-\frac{(\mathbf{r}-\mathbf{r}_0)^2}{\sigma^2}} e^{i(\mathbf{kr}-\omega t)}$$

where:

$\psi(r) = \psi_+(r), \psi_-(r)$ are the two circular components of the photon wave function (polariton polarization)
m is the cavity photon (polariton) mass
U describes the honeycomb lattice
τ is the lifetime of photon (polariton)
β-term describes L-T splitting

Numerical simulation

- To check the validity of TB approximation and observability of the OSHE in real samples, they solve the equation of motion for photonic spinor

$$i\hbar\frac{\partial\psi_\pm}{\partial t} = -\frac{\hbar^2}{2m}\Delta\psi_\pm + U\psi_\pm - \frac{i\hbar}{2\tau}\psi_\pm + \tag{5}$$
$$+\beta\left(\frac{\partial}{\partial x} \mp i\frac{\partial}{\partial y}\right)^2\psi_\mp + P_0 e^{-\frac{(t-t_0)^2}{\tau_0^2}} e^{-\frac{(\mathbf{r}-\mathbf{r}_0)^2}{\sigma^2}} e^{i(\mathbf{kr}-\omega t)}$$

where:

$\psi(r) = \psi_+(r), \psi_-(r)$ are the two circular components of the photon wave function (polariton polarization)
m is the cavity photon (polariton) mass
U describes the honeycomb lattice
τ is the lifetime of photon (polariton)
β-term describes L-T splitting
P_0-term describes linearly polarized light (during time τ_0) exciting a wavepacket at point $\mathbf{k}$ and around $\mathbf{r_0}$

Numerical simulation

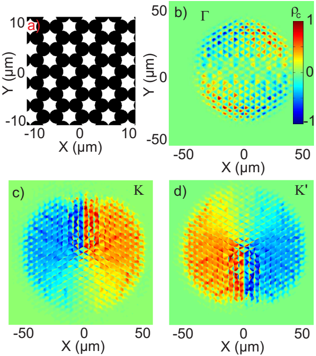

Figure : OSHE in photonic graphene. Circular polarization degree as a function of coordinates: a) the potential used in the simulations; b) excitation at Γ point (TE-TM field); c) excitation at K point (Dresselhaus effective field); d) excitation at K' point (field inverted with respect to K').

Their conclusions

- They studied the SOC induced by the L-T splitting in a microcavity etched in the shape of a graphene lattice.

Their conclusions

- They studied the SOC induced by the L-T splitting in a microcavity etched in the shape of a graphene lattice.

- Within the tight-binding approximation, they found the eigenstates of the system, derived an effective Hamiltonian and found the effective fields acting on the photon spin.

Their conclusions

- They studied the SOC induced by the L-T splitting in a microcavity etched in the shape of a graphene lattice.

- Within the tight-binding approximation, they found the eigenstates of the system, derived an effective Hamiltonian and found the effective fields acting on the photon spin.

- The symmetry of the field is lowered close to the Dirac points where it takes the form of a Dressehlauss field.

Their conclusions

- They studied the SOC induced by the L-T splitting in a microcavity etched in the shape of a graphene lattice.
- Within the tight-binding approximation, they found the eigenstates of the system, derived an effective Hamiltonian and found the effective fields acting on the photon spin.
- The symmetry of the field is lowered close to the Dirac points where it takes the form of a Dressehlauss field.
- They verified the experimental observability of the optical Spin Hall effect induced by this spin-orbit coupling by numerical simulations.

Nature Physics 10, 803813 (2014) doi:10.1038/nphys3143

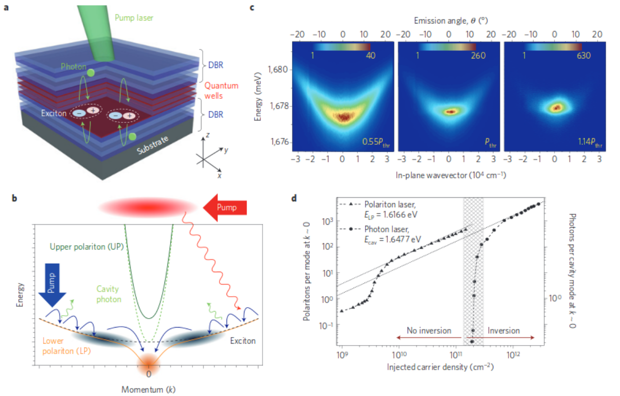

Figure 1 | Exciton-polariton condensation. a, Typical device structure supporting exciton-polaritons. Excitons, consisting of a bound electron-hole pair, exist within the quantum well layers. These are sandwiched by two distributed Bragg reflectors (DBRs), made of alternating layers of semiconductors with different refractive indices. The DBRs form a cavity that strongly couples a photon and an exciton to form an exciton-polariton. Polaritons are excited by a pump laser incident from above. **b**, Exciton-polariton dispersion and condensation process. Strong coupling between the cavity photon and exciton dispersions split the dispersions near $k = 0$ to create the lower polariton (LP) and upper polariton (UP) dispersions. The pump laser initially excites high-energy excitons, which then cool via phonon emission towards the bottleneck region (black clouds). We show both the resonant pumping scheme (large blue arrow) and the non-resonant pumping scheme (large red arrow, pumped at a higher energy beyond the scale shown). Excitons in the bottleneck region then scatter into the condensate (orange cloud) via stimulated cooling. **c**, Experimental dispersion images of polariton condensate formation from ref. 5. Below the threshold for condensation the polaritons are broadly distributed in momentum and energy. At and above threshold the polaritons condense in the $k = 0$ ground state. **d**, Polariton ground state population for a polariton laser as a function of the pump power from ref. 36. The figure also shows the threshold for a standard laser achieved by a sufficiently large detuning to lose strong coupling in the same sample for comparison.